ELEVENTH EUROPEAN ROTORCRAFT FORUM

Paper No. 5

BLADE/VORTEX INTERACTIONS AND NOISE ABATEMENT TECHNIQUES DURING DESCENT

John Pollard

Westland Helicopters Ltd.
Yeovil, England.

September 10-13, 1985
London, England

THE CITY UNIVERSITY, LONDON, EC1V OHB, ENGLAND

BLADE/VORTEX INTERACTIONS & NOISE ABATEMENT TECHNIQUES DURING DESCENT

by

J.S. Pollard

WESTLAND HELICOPTERS LTD.

ABSTRACT

The advent of international noise regulations for civil helicopters and the increasing sales competion in the heliport route market has highlighted the need to reduce helicopter noise during take-off, flyover and approach phases. In particular, manufacturers the world over have embarked on major programmes to reduce or control the impulsive blade slap noise characteristic of the descent condition.

There are two basis sources of impulsive noise - compressibility effects resulting from high advancing blade tip Mach numbers, and blade vortex interactions in the main rotor disc region. The latter is the subject of this paper and is associated with interactions between the main rotor blades and their own wakes. It occurs at those flight conditions where the vortex wake can be expected to pass close to the rotor, primarily partial power descents and banked turns. The degree of blade slap produced is dependent on the rate of descent and significant variations in impulsive noise content have been measured for a wide range of descent angle/forward speed combinations with, in WHL experience, the standard ICAO certification 6°/70 knot condition giving the highest noise level. Under conditions of severe slap, increases in the noise level of 8 dBA have been measured and this type of noise is readily detectable over considerable distances.

This paper describes the investigations conducted by Westland Helicopters Limited, to provide a fundamental understanding of the blade slap mechanism and to recommend noise abatement procedures for Flight Manual operation.

1. INTRODUCTION

In flight measurements on the W-30 helicopter have shown that certain combinations of speeds and descent angles are more prone to blade slap noise than other approach conditions. This is illustrated in Figure 1 and clearly for this helicopter the dBA curve peaks at descent rates around 800 - 1000 ft/min. Also, although the values are based on the average of three microphone positions (centreline and two sideline), they exhibit a large degree of scatter for a given condition. A closer examination of these results shows lines or curves of constant descent angle or constant speed. The latter (Figure 2) gives straight line relationships of noise versus descent rate at constant forward speed with the gradient changing as speed increases, and indicates how sensitive noise is to both speed and angle. Nominal descent rates and not actual descent rates are shown on figures 1 and 2 and these differences are discussed later.

The shape of the noise versus speed curves show marked similarities with early but crude aerodynamically derived blade slap boundaries from simple uniform downwash models. Blade slap noise is likely to be a maximum when the main rotor tip vortices stay in the disc plane, and based on the established average downwash at the disc this results in an equality of the form

$$\frac{C_T}{4} \simeq \left(\mu_z + \frac{n\,c}{2\,\pi\,R} \right) \mu_x$$

where C_T = thrust coefficient, μ = advance ratio, n = integer and c = chord.

For nominal values of thrust of 12,000lb, tip speed of 770ft/sec. and for n = 0, the centre curve of Figure 3 is obtained and this represents the range of Vx and Vz conditions for which the vortices stay in the disc plane. This curve has a similar shape to the dBA versus Vx curves with asymptotic tendancies at increasing Vx and increasing Vz. Furthermore, a 'width' can be provided to the theoretical curve by allowing vortices to be displaced 1 or 2 chords from the disc plant (n = 1, -1 etc). This results in other curves displaced from and parallel to the centre curve (Figure 3) but with increasing displacement along the lines of constant angle. For comparison Figure 3 contains an approximate measured blade slap boundary, and clearly the theoretical curves run through the measured boundary. Whilst the uniform downwash theory is only a crude model, it is nevertheless encouraging enough to explore further and consequently the WHL Aerodynamics Department embarked upon extensive unsteady airfoil theories to predict the vortex wake pattern and blade/vortex interaction loadings.

2. AERODYNAMIC MODELLING

The reader is referred to references 1 and 2 for a detailed account of the basic theory, but the important steps are outlined as follows :-

A method for calculating the time dependent loads arising from a blade/vortex encounter has been developed using the concept initially of an infinite straight wing parallel to a straight line vortex convecting past. The model was then refined to account for (i) finite blade size, (ii) curved vortex path, which affects induced velocities and the progression of the intersection point along the blade, (iii) a radial velocity gradient along the blade, (iv) a non uniform downwash field and (v) wake distortion caused by the downwash. The wake geometry was modelled by considering each turn of the spiral trailing vortex path and defining the relative positions of vortex and blade portion under consideration. The induced velocity on the blade together with the resultant induced loading were then calculated. The latter consists of a circulatory component obtained by an indicial response function of a rotor loads model and a more dominant impulsive contribution obtained from modified piston theory. All these parameters are required to generate blade loadings at 24 radial stations (from 40% blade radius to the tip) and 720 azimuth angles (every $\frac{1}{2}°$) so that all forms of intersection (tangential, skew etc) on both advancing and retreating blades are covered. Such large resolution is required to accurately define the downwash and provide very high sampling values for the very narrow impulsive noise signals generated.

3. ACOUSTIC PRESSURE FORMULATION

The procedure for convering blade loading data during blade/vortex interactions to acoustic pressure pulses has been derived by the WHL Theoretical Studies Department (ref.3). The theory basically takes the dipole term in the Lighthill wave equation which gives the acoustic pressure at point x and time t as

$$4\pi p(x, t) = \frac{\partial}{\partial x_i} \int \left[\frac{f_i(y, \tau)}{r(1 - M_r)} \right] dy$$

where $f(y,\tau)$ is the localised lift force per unit area on the blade at a given time and $r = x - y(t)$ is the distance between source and observer. This integrand needs to be evaluated for the lift variation with azimuth along the blade radius and at the appropriate retarded time factor. The latter arises because of the Doppler shift in frequency between the source and receiver and because of the fact that the sound generated by separate points on the blade radius will arrive at the observer point at slightly different times.

Assumptions are made that only the force f in the lift direction is important, that the blade chord is sufficiently small to ignore retarded time differences across the chord and that the observer must be positioned in the far field. This last condition means that the theory can not yet be applied to near field microphone positions mounted on the helicopter itself. After taking these assumptions into account the basic expression becomes :-

$$p(x,t) = \frac{-\cos\mu}{4\pi r_o a_o} \quad \frac{\Omega}{(1 - M_{or})} \quad \frac{\partial}{\partial\alpha} \int \left[\frac{l(R,\psi)}{(1 - M_r)} \right] dR \qquad (1)$$

where M_{or} and M_r are mach number terms, μ = observer angular position, Ω = rotational speed.

$$\alpha = \frac{\Omega\,(t - r_o/a_o)}{(1 - M_{or})} \quad \& \quad l(R,\psi) \text{ is the blade loading}$$

values at discrete values of radius R and azimuth ψ.

Owing to the retarded time factor α, the blade loadings at each radial and azimuth position are not in phase relative to an observer in the far field. Consequently the blade loadings have to be integrated along lines of constant α before the impulsive pressure waveform is calculated. This effect is illustrated in figure 4, where the dotted lines curving out from the hub centre (from 0.4 blade radius to the tip) represent lines of in-phase components relative to the observer. The case shown is for an observer located 1000ft ahead of the helicopter at 1000ft altitude. The curvature is very pronounced over a wide range of azimuth angles but changes in direction depending upon whether the observer is located on the retreating side (fig. 4(a)) or the advancing side (fig. 4(b)). Finally the thickness noise component is added to the blade slap signal (if required) and the signal is modified to account for more than one blade.

4. GROUND REFLECTION EFFECTS

The measured data is, unfortunately, contaminated by ground reflection effects owing to interference between the direct and ground reflected waves for the 1.2 metre microphone. This results in interference effects in both the frequency and time domains which complicate the measured waveforms. A computer program has, therefore, been developed for correcting predicted waveforms to allow for ground reflection changes. It is based on theory developed by ESDU for correcting data in the frequency domain by applying it to the time domain so that the reflected waveform and hence the combined waveform can be predicted for a given theoretical direct wave. The basic effect is to double the number of impulses in a group with the relevant amplitudes and spacing between each pair of pulses dependent on the source/observer distance and the ground surface. Figure 5 illustrates the effect of changing microphone height on an idealised pulse. For the 0.01m height (i.e. microphone embedded in ground surface) there is an amplitude doubling of the signal with very little phase shift, but at the other extreme of a 10m mast mounted microphone the reflected pulse is so far shifted from the direct pulse that it will interfere with a later pulse from another blade.

5. MODEL VERIFICATION

The acid test for any theoretical model is firstly its correlation with measured data and secondly its ability to predict parametric design changes. The present model is still being developed and requires verification, but success in the long term enables the source noise mechanisms to be fully understood and provides guidelines for future noise reductions. In the short term WHL have concentrated on the important certification and operational issues of selecting descent procedures for minimum noise impact. Since currently flight tests have shown the 6° glide slope/70 knot speed combination to be one of the noisiest and most variable conditions, the effect of descent rate changes at constant speed have been explored both in terms of blade slap boundary mapping over a range of nominal descent angles and the complications introduced by flying down a supposedly constant 6° glide slope. The 6°/70 knot descent has been taken as the datum condition, because this represents the certification test condition imposed by ICAO regulations. Before discussing the effects of changing descent rate, the characteristics of the datum condition are examined first.

Datum Condition

With the forward speed fixed at 70 knots, the horizontal separation of blade and vortex is independent of descent speed and Figure 6 shows the predicted loci of possible intersections of blade and vortex as viewed from above the rotor. The vertical separation will change with descent rate, however, and only a few of the interactions shown will occur or be dominant, for a given rate of descent. For the 6° angle or 740 ft/min. datum case the vortex path from blade 3 produces an intersection in the first quadrant (advancing side) at an azimuth angle of about 40° and near the blade tip. A retreating blade intersection in the last quadrant is also predicted to occur, but this is not thought to be significant.

A comparison of measured and predicted peak pressure time histories becomes exceedingly complex because of a number of interrelated problems. For example as the helicopter flies towards and over the ground microphone positions, the amplitude and duration of the measured impulses change due to directivity effects, Doppler shift and the decreasing slant distance between source and receiver. These change with descent angle and speed and between sideline and under the flight path microphones. Also there is a time delay between when the noise is emitted at source and when it is received on the ground. Consequently it is very difficult to select a particular time window for evaluation between different measurement conditions and for comparison with predicted data. Equally the predictions have shown themselves to be highly sensitive to small changes in rotor parameters, observer location etc. Until these issues have been fully investigated, a more general appraisal of waveform shapes and amplitudes is more appropriate at this point in time.

Figure 7 illustrates a typical predicted pressure time history for a 4 bladed rotor with advancing side interactions. The thickness noise contribution has been added using an idealised waveform to show its position relative to the blade/vortex interaction pulse. Finally Figure 8 shows the result of including ground reflections. Typical measured data for three different descent conditions is presented in figure 9 and clearly, in comparison, the predicted results are very promising. It should be noted that previous comparisons in reference 2 are in error in that the predicted pressure amplitudes should be reversed in sign.

Directivity Patterns

A combination of factors in the acoustic pressure formulation (equation (1)) results in unusual directivity characteristics. Firstly the presence of the blade mach number means that interactions near the blade tips are more acoustically efficient and advancing blade interactions are more intense than retreating ones.

This latter effect may overcome any tendency for higher blade loading components on the retreating side. Secondly, regardless of where the blade is positioned during an interaction the Doppler factor results in the maximum noise position being observed 90° azimuth in advance of the blade position. Thus impulsive interactions on the advancing side and first quadrant tend to throw the noise forwards and to the starboard side, whilst retreating blade interactions direct the noise rearwards. Clearly if a change in descent condition results in a change in azimuth interaction angle, then a change in directivity pattern will occur and this suggests that there is no fixed in-plane directivity pattern for all descent conditions. In addition the cos μ term ourside the integral of equation (1) affects the out of disc plane directivity pattern and the combined effect is an approximate predicted lobed shaped pattern above and below the rotor disc plane.

Taking the 6°/70 knot datum condition, the predicted 3-dimensional directivity plot relative to the aircraft is shown in Figure 10. Since the dominant blade/vortex interaction is predicted to occur at 40° azimuth and 1.OR, the maximum noise is radiated approximately 45° below the disc plane ahead of and on the starboard side of the helicopter.

These predicted lobe shaped patterns are not entirely consistent with measured data, since although the starboard positioned microphone correctly registers higher noise levels than the port side, the centre microphone time histories indicate peak noise closer to aircraft overhead (i.e. 60-90° below disc plane) than the predicted 40-45°. Also the increase in number of blade/vortex interactions seen on the side line microphone traces, relative to the centre line traces, suggests these positions are picking up both retreating and advancing blade interactions.

6. BOUNDARY MAPPING

According to measurements certain combinations of forward speed and descent angle are more prone to blade slap noise and Figure 2 indicated lines of constant speed whereby dBA levels increased with increasing descent rate. According to the rotor wake model, changes in descent rate result in critical changes in vertical separation between blade and vortex and in order to evaluate this further the interaction positions were predicted for a range of descent rates (416-1109ft/min) at a constant 70 knots forward speed. The results are presented in Table 1 for the advancing side interactions only. With a 4 bladed rotor (denoted blades 0-3 in sequence), each blade will deposit a vortex trail near the rotor disc and Figure 6 defines the azimuth angles over which interactions are possible between a later blade and a vortex 1 - 2 revolutions old. As blade 0 rotates there will be a critical value of advance ratio μ_z at which the main interaction occurs and above or below these μ_z values the vortex will either pass above or below the blade. At the nominal 6°/70 knot condition (i.e. 740 ft/min descent rate) a tip intersection occurs with a vortex from blade 3 at 40° azimuth. As the descent rate and hence μ_z decreases, the main intersection moves to a larger azimuth angle with a vortex from a different blade. Thus at 600 ft/min blade 2 vortex experiences a parallel tangential interaction at $\psi = 50°$ and 0.8R, whilst the previous vortex from blade 3 no longer gives so intense an interaction because the vortex has moved below blade 0. Similarly at a higher descent rate (878 ft/min) blade 0 experiences an interaction at $\psi = 25°$ and 0.8R with its own vortex (generated one revolution earlier), whilst the blade 3 generated vortex has now moved above blade 0. The predicted vortex trajectories for each of the critical advance ratios μ_z are shown in Figure 11 in both plan and side view. The points of intersection in terms of azimuth angle and blade position are clearly illustrated. Also of interest is the way the vortex trails curl upwards near the blade tips as a result of descending flight.

The impulsive noise produced is dependent on the changes in blade loading associated with all the intersections taking place and the prediction program generates the blade loading values for every $\frac{1}{2}°$ azimuth change and 24 radial stations. Consequently it is not necessarily true that one dominant intersection

will result in high noise levels, other intersections may contribute. Peak pressure waveforms have been predicted for the different descent rates and a few are shown as inset diagrams on Figure 12. These represent one blade signatures only with no thickness noise contributions and no ground reflection corrections, and the ground observer is positioned in turn at the three standard measuring positions relative to the helicopter at 406 ft altitude. The centreline and starboard positions detect advancing blade interactions, but the port side line position is clearly picking up pronounced retreating blade interactions. The rms amplitudes of all the waveforms have been used to derive the noise versus descent rate plot of Figure 12. The shape of the curves is not too dissimilar from the measured dBA data of Figures 1 and 2, bearing in mind that the predicted curves are for constant 70 knots forward speed and the measured data is based on nominal descent rates and not actual descent rates as discussed in the next section.

7. NOISE LEVEL VARIABILITY

Measured noise levels for the descent condition are subject to large variations between nominally identical conditions. During certification trials of the W-30, six repeat runs of the ICAO 6°/70 knot condition showed 7 dBA variation in peak noise level at the centreline position. The difficult requirement for the pilot to fly down a constant glide slope at constant speed results in small but rapid changes in rotor operating parameters and consequent excursions in and out of blade slap regimes. In the WHL tests a precision approach path indicator was used to define the glide slope with the pilot required to fly within the narrow light beam. Whilst the procedure controlled the aircraft position well (Figure 13), the descent rate as measured by kinetheodolite equipment, varied considerably down each flight path (Figure 14). A closer examination of these two figures explains what is happening. For example, in the case of run 305, the pilot joins the glide slope whilst still climbing (Figure 13). He then has to alter his rate of descent rapidly (Figure 14) to stay within the PAPI beam and eventually reaches the microphone position with a descent rate of about 900 ft/min well above the 740 ft/min nominal value. Similar explanations exist for the other runs and even run 307, which is almost exact for aircraft position, has descent rate variations between 500 and 740 ft/min. Forward speed is not constant either and typically varies by 5 per cent.

Clearly whilst precision flying has occurred in terms of aircraft position, the rate of descent has varied on average by a factor of 3, with consequent large changes in measured noise level at the overhead position and varying degrees of blade slap radiation down the flight path. It is, therefore, believed that the presence of approach guidance systems to assist flight path definition is in fact adding to the noise problems.

Attempts are being made to correlate the changes in noise level during a given descent with the changes in descent rate. This requires accurate synchronisation of noise data with kinetheodolite data after taking into account Doppler time shifts. Since the noise levels automatically increase as the source/observer distance gets smaller, it is necessary to remove the distant effects from the noise time histories. The crest factor unit, used to illustrate the impulsive content of noise signals, provides the answer since by definition it subtracts the average noise level from the peak noise level and is, therefore, almost independent of distance. The crest factor descriptor found to be particularly sensitive to blade slap noise on the W-30 was $\frac{\text{LIN PEAK}}{\text{LIN RMS SLOW}}$ where LIN PEAK and LIN RMS SLOW are the peak level and RMS Slow level respectively of the unweighted signal. Crest factor analysis was, therefore, performed on runs 302 to 307 of the 6°/70 knot condition and the resulting time histories were compared with the rate of descent traces corrected for receiving time instead of emission time. Figure

15(a) shows the crest factor time history for run 304 and fig.15(b) correlates the crest factor level with descent rate over this 20 sec. time period. The results are not very conclusive in that one would hope to see the data points collapse to a hump shaped curve similar to figure 1. Unfortunately, the ground reflection effects are causing signal distortions throughout the noise time history and it is difficult to ascertain whether fig.15(b) is showing any clear trends or not. Further research is continuing in this area.

Returning to the measured data presented in Figures 1 and 2, it is clear that the use of nominal descent rates is incorrect and the figures should be revised for actual descent rates close to overhead. Unfortunately kinetheodolite data is not available for all the angles and speeds tested and it is, therefore, not possible to determine the true descent rate of each condition. An approximation can, however, be obtained by using the measured descent rates close to overhead for runs 302 to 307 of the 6°/70 knot condition of figure 14. The resulting dBA noise level versus descent rate plot for the three microphone average is given in Figure 16, and two points of interest emerge. Firstly the dBA noise variation with rate of descent shows the same characteristic hump shape as Figure 1 and secondly the apparent variability in noise level of the nominal 6°/70 knot condition has now been reduced by taking into account actual descent rates. This has very important implications for both noise certification tests and noise abatement procedures.

8. NOISE ABATEMENT PROCEDURES

As a result of experience gained in mapping out the blade slap boundaries, it is possible to select descent procedures for minimum noise impact, but still be commensurate with recognised safety procedures and passenger comfort. In heliport situations where there are no restrictions of fixed glide path angles, low noise approaches are best served by low speed/low angle combinations or high speed/high angle combinations, as indicated by Figures 1 and 2. In the former case low speed combinations, e.g. $4\frac{1}{2}$°/30 knots, are not desirable because of the longer times taken to pass over the community and the difficulties of maximising the power margins in the event of engine failure and meeting the landing decision point (LDP) of 60 knots at 100 ft altitude. In the latter case high forward speeds overcome the community exposure time problem and high rates of descent are believed acceptable to passengers provided that the transitions from level flight to descent and from descent to the LDP are conducted smoothly. In the case of the W-30, trials at a descent rate of 1250 ft/min. and 100 knots forward speed have resulted in significant noise benefits and passenger acceptability. Figure 1 illustrates these noise abatement approaches and shows a benefit of about 7 dBA (3 microphone average) over the worst descent conditions. During flying the pilot is requested to hold the high rate of descent and high forward speed as long as possible down the flight path before reducing speed and descent rate to pass through LDP. This is important in that, although this speed/descent rate combination equates in theory to a fixed angle of 7°, the pilot does not have to concentrate on flying to a fixed glide path. This noise abatement procedure has now been incorporated in the helicopter flight manual with a recommendation that it is used in practice.

In heliport situations where there are restrictions such as fixed glide paths, then it is still possible to reduce the noise exposure by allowing the pilot to fly in a smooth manner (less pilot control inputs) and sticking to rates of descent which minimise blade slap.

9. CONCLUDING REMARKS

The completion of the aerodynamic blade loading model of the blade/vortex interaction process has enabled peak pressure time histories to be predicted for the descent condition. Initial correlation with measured data is promising leading to a greater understanding of the noise source mechanisms, the associated noise level variability and the flight boundaries of operation. Findings to date suggest descent noise can be reduced by attention to pilot flying techniques and by adopting noise abatement procedures. Operational guidelines have now been incorporated in the helicopter flight manual and should go some way to assist the worldwide fly neighbourly objectives of the helicopter industry.

10. ACKNOWLEDGEMENTS

The author wishes to thank his colleagues in the Acoustics, Theoretical Studies and Aerodynamics Departments who have provided invaluable assistance in the preparation of this paper. In particular T.S. Beddoes was responsible for the blade loading aerodynamics model and A.C. Pike and M.A. Reed were responsible for the computer program development for the acoustic pressure predictions and waveform analysis. The Ministry of Defence is also acknowledged for its financial support under MoD contracts.

11. REFERENCES

1. T.S. Beddoes — A wake model for high resolution airloads. US Army/AHS International Conference on Rotorcraft Basic Research. February 1985

2. T.S. Beddoes — Unsteady Aerodynamics. Application to Helicopter Noise and Vibration Sources. AGARD Symposium on Unsteady Aerodynamics Gottingen. May 1985.

3. D.L. Hawkings — Theoretical Analysis of Blade/Vortex Interaction Noise. WHL AA Note 1417 1984.

RATE OF DESCENT (FT/S)	μz	VORTEX POSITION/CRITICAL AZIMUTH				CRITICAL INTERSECTION POINT	AGE OF VORTEX (REVS)	TYPE OF INTERSECTION
		BLADE 0	BLADE 1	BLADE 2	BLADE 3			
6.93	0.009	BELOW	60°	BELOW	BELOW	0.6 R	1	ACUTE
10.00	0.013	BELOW	ABOVE	50°	BELOW	0.8 R	1¼	PARALLEL
11.55	0.015	BELOW	ABOVE	ABOVE	BELOW	-	-	-
12.71	0.0165	BELOW	ABOVE	ABOVE	40°	1.0 R	1½	ACUTE
14.63	0.019	25°	ABOVE	ABOVE	ABOVE	0.8 R	1½ - 1¾	OBLIQUE
18.48	0.024	ABOVE	ABOVE	ABOVE	ABOVE	-	-	-

OTHER INTERSECTIONS NOT COVERED : BLADE 0 AT $\Psi \approx 70°$ & BELOW 0.009 μz
BLADE 3 AT $\Psi \approx 75°$ & BELOW 0.009 μz

TABLE 1 EFFECT OF DESCENT RATE ON INTERSECTION CHARACTERISTICS AT 70 KNOTS FORWARD SPEED

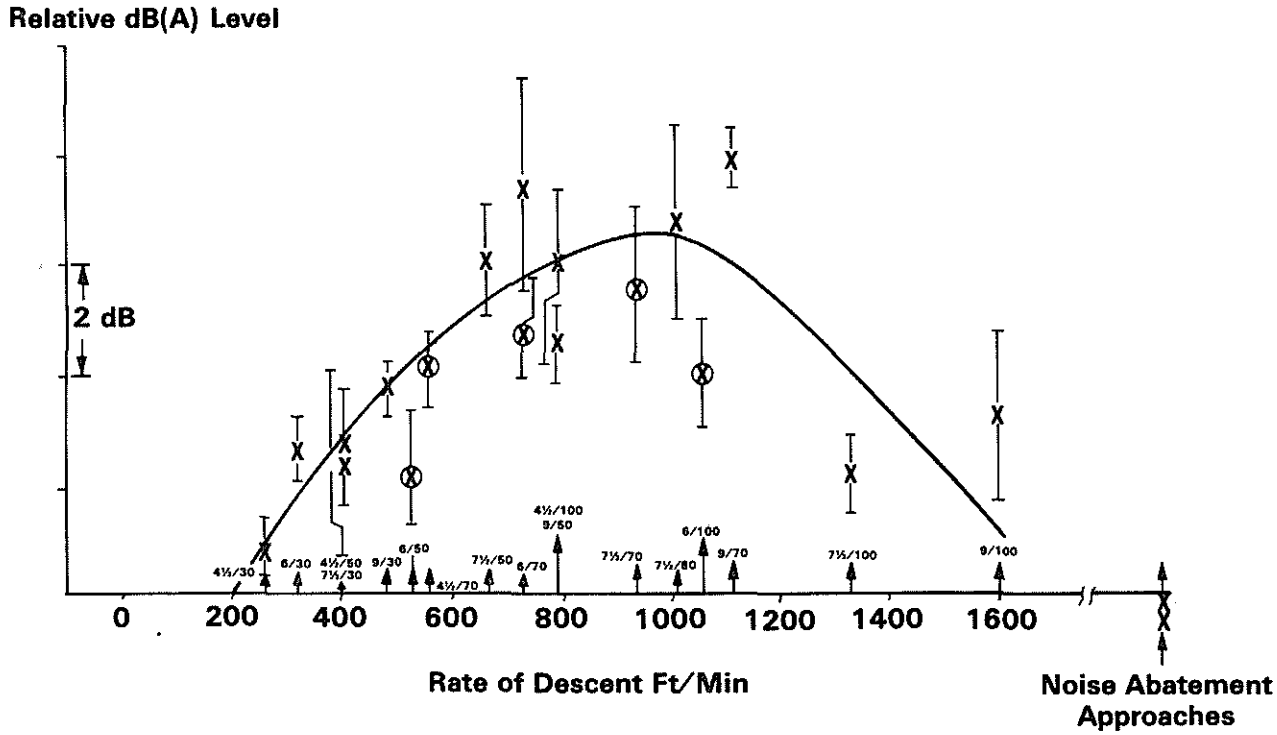

Figure 1 Approach Noise Versus Rate of Descent

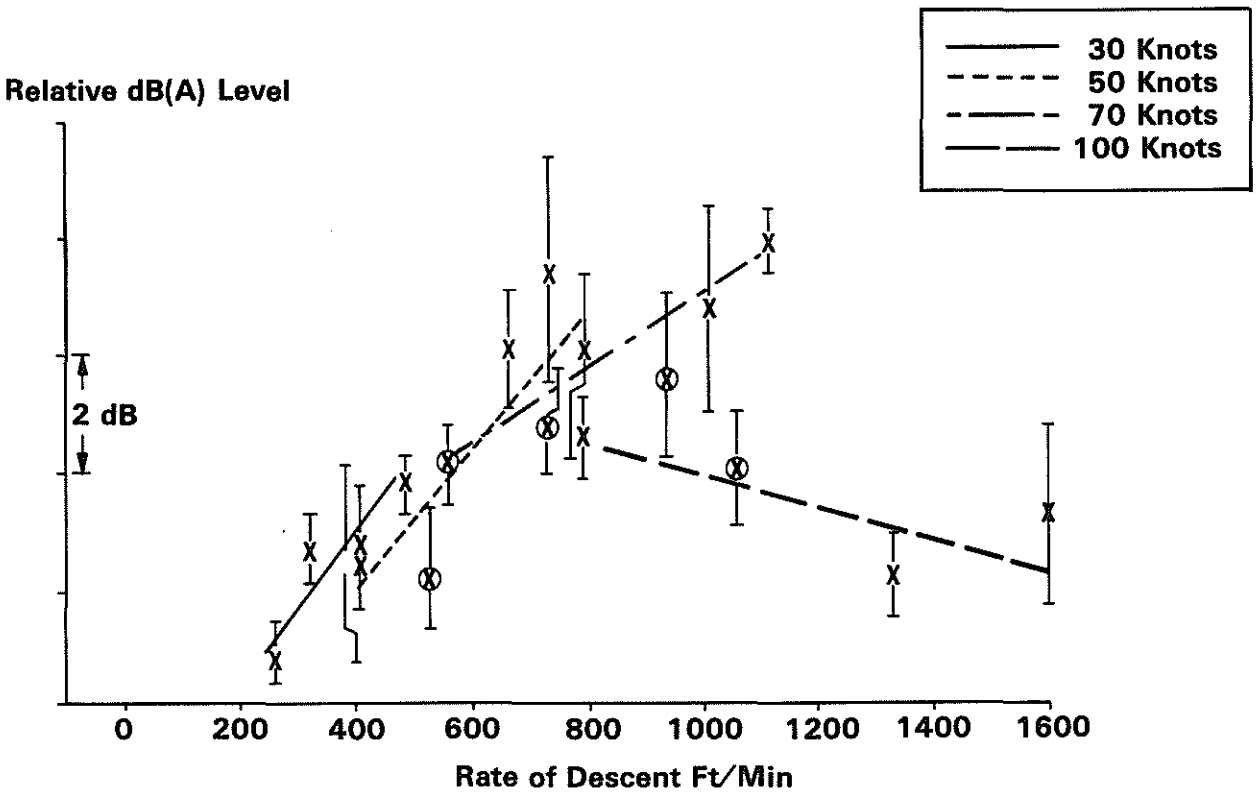

Figure 2 Lines of Constant Speed

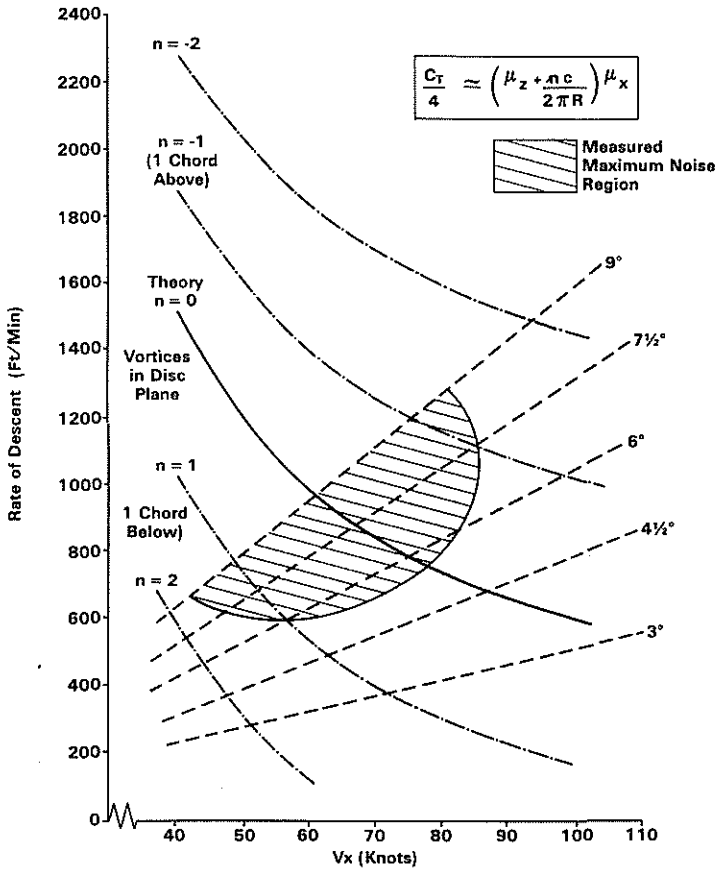

Figure 3 Theoretical Blade Slap Boundaries Using simple Downwash Theory

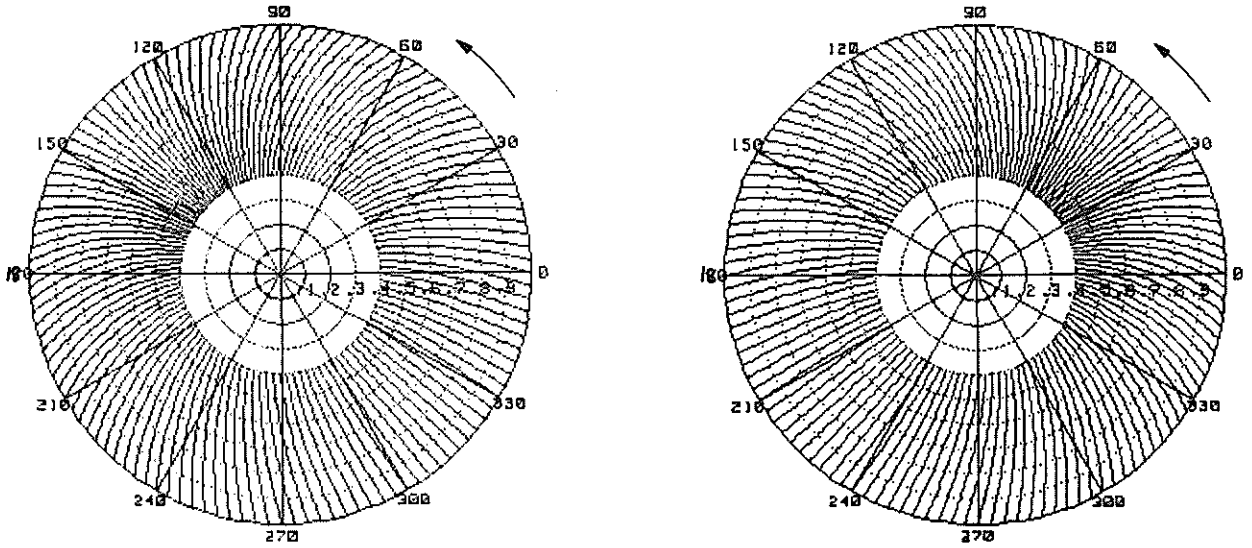

(a) Observer on Retreating Side

(b) Observer on Advancing Side

Rotation Direction

Alt = 1000 ft

Side = 1000 ft

Dist = 1000 ft

Flight Path

Alt = 1000 ft

Side = 1000 ft

Dist = 1000 ft

Figure 4 In-Phase Source Positions in Rotor Disc Plane (Integration Along Lines of Constant $\propto$)

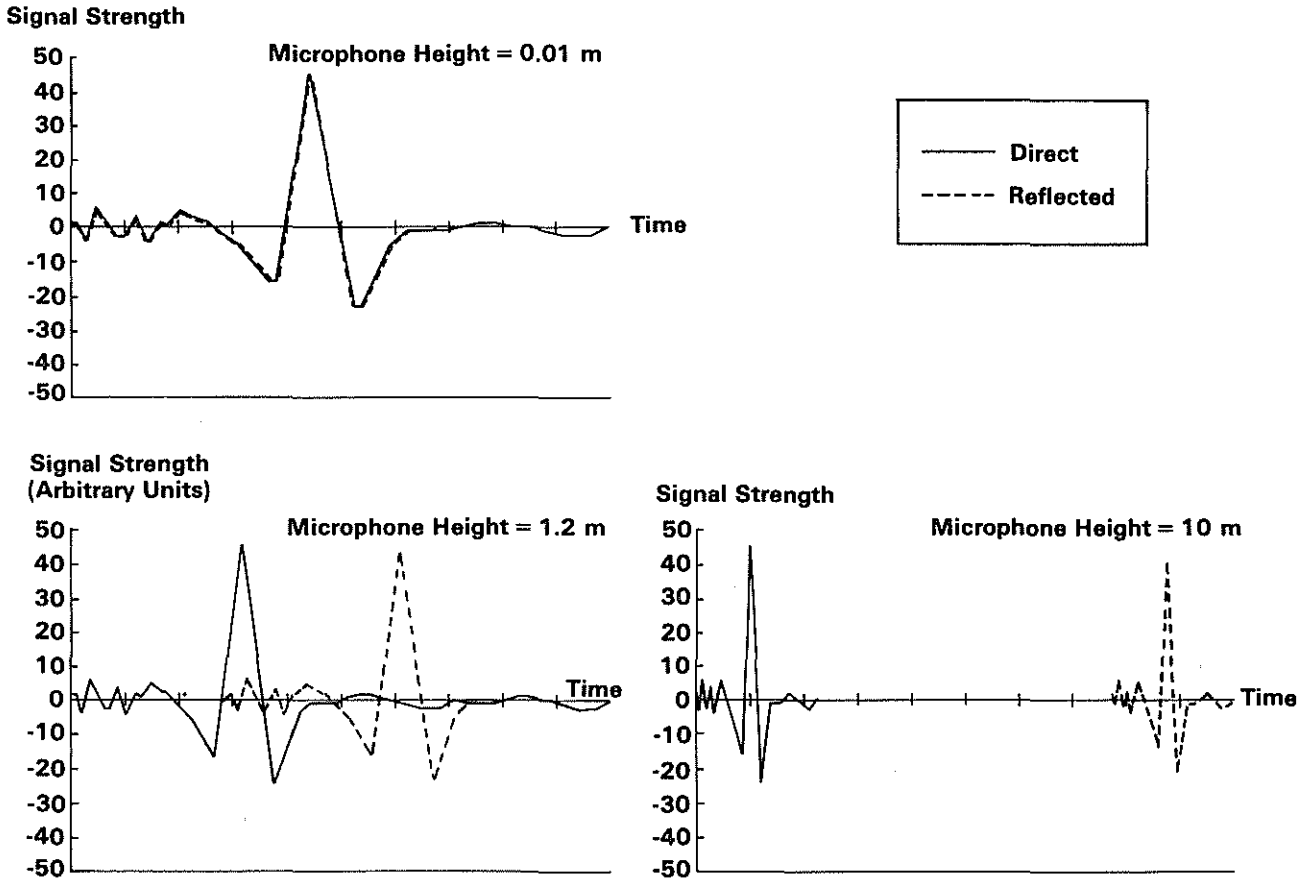

Figure 5 Effect of Microphone Height (Hard Ground Source)

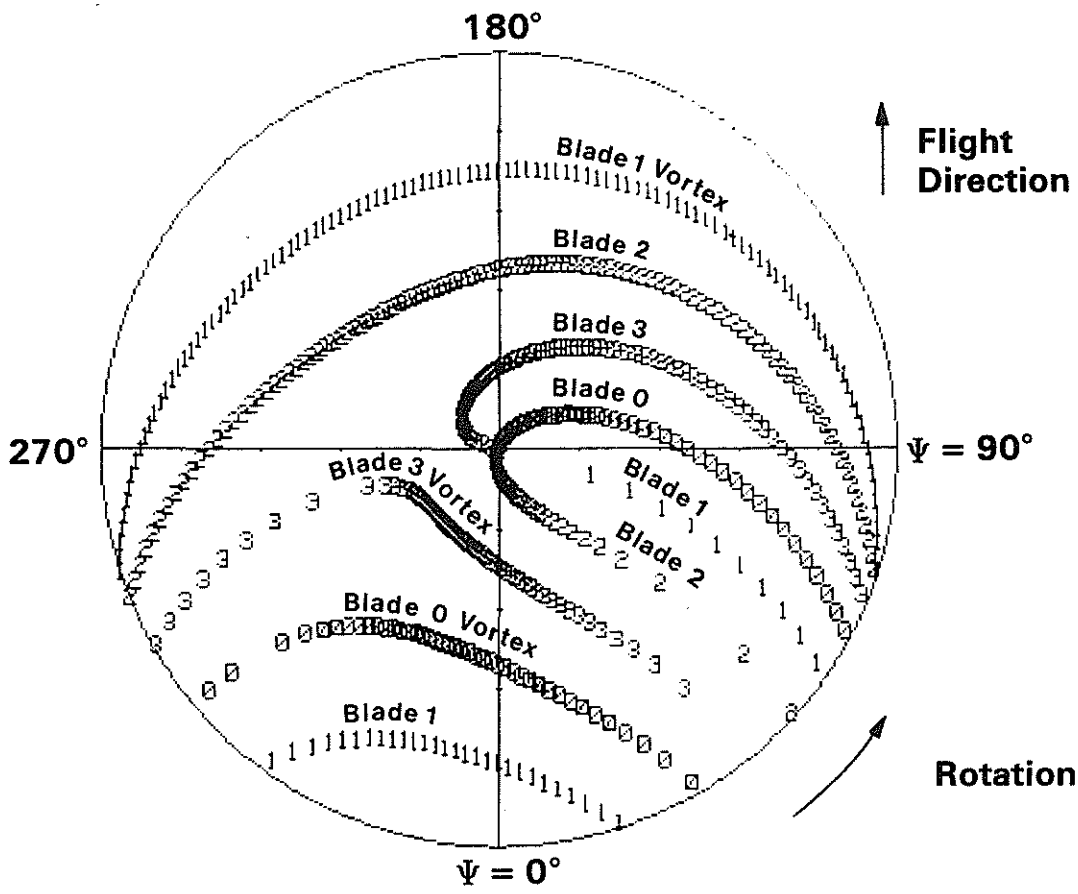

Figure 6 Blade/Vortex Loci of Intersections in Disc Plane at 70 Knots Forward Speed

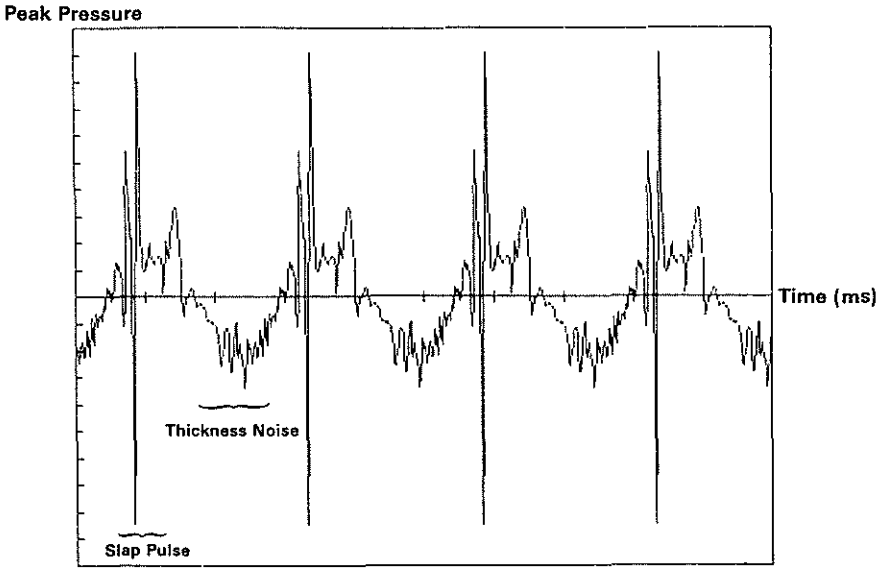

Figure 7 Typical Predicted 4 – 'Bladed Slap & Thickness Noise' Waveform

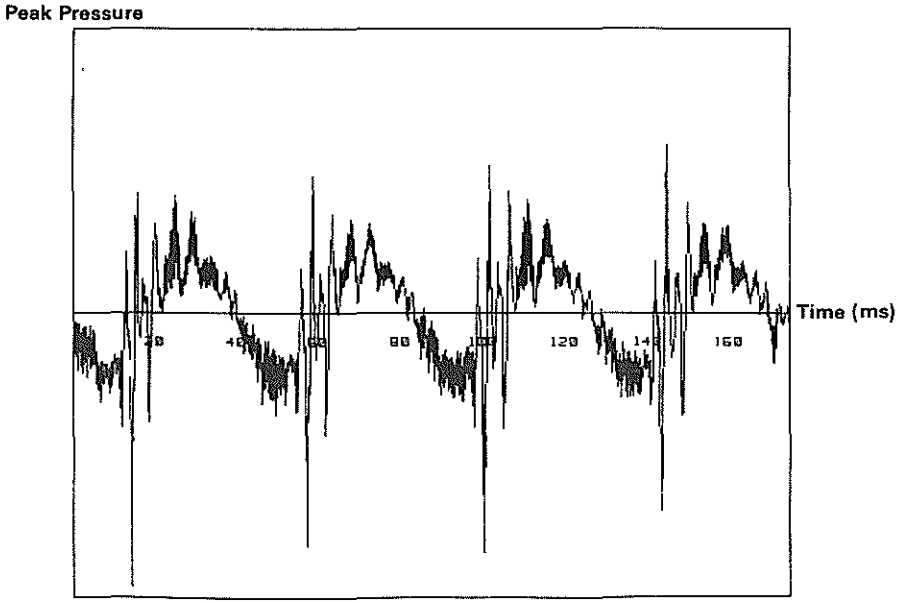

Figure 8 Typical Predicted Ground Reflected Waveform

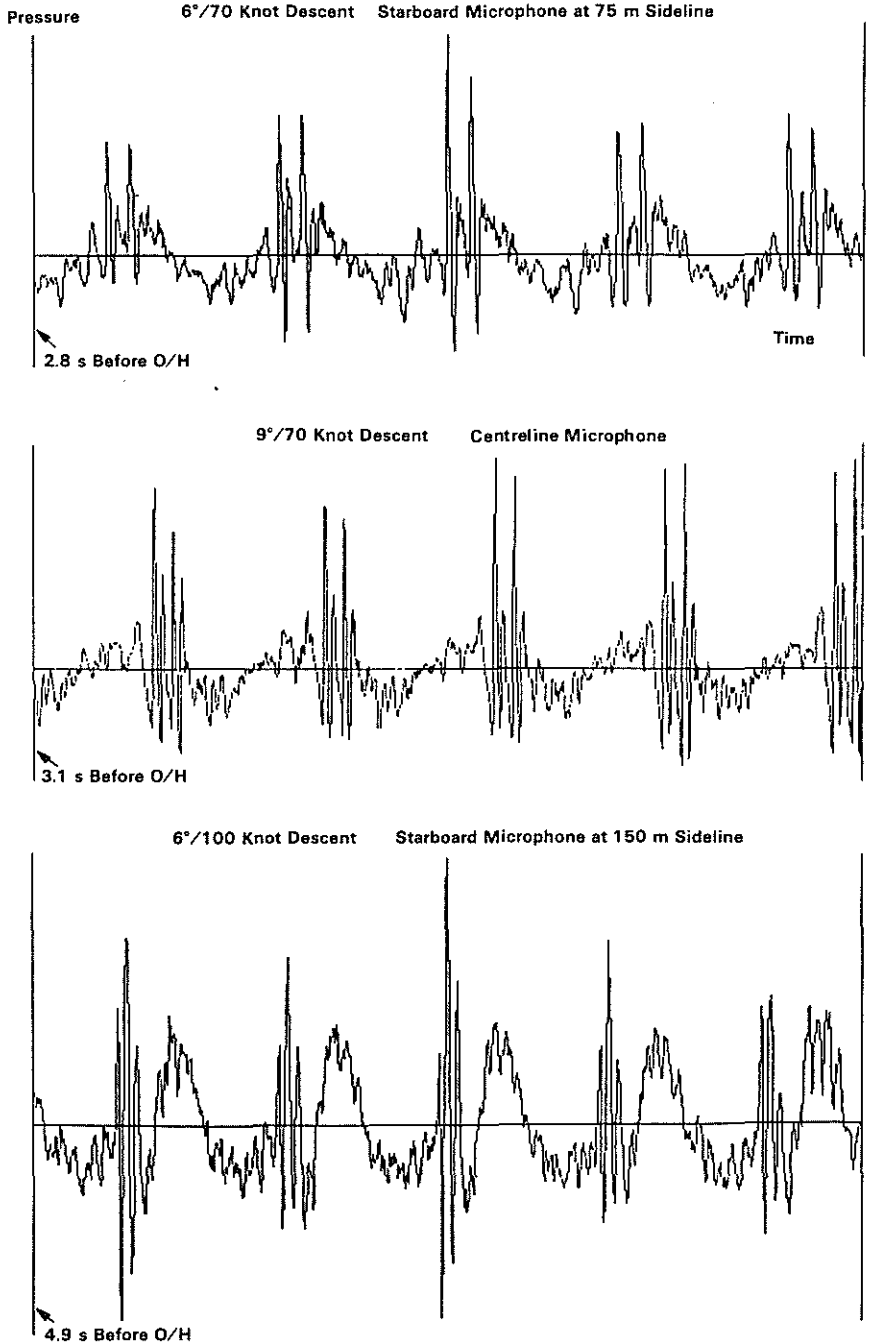

Figure 9 Measured Peak Pressure Time Histories (0.2 s Trace Length)

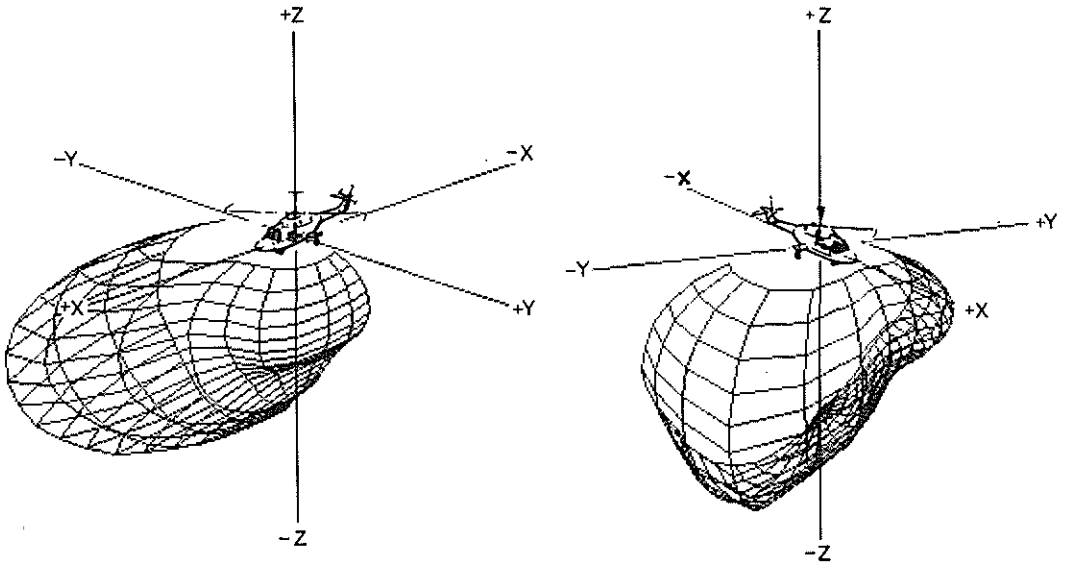

dB Contour Relative to Aircraft (Rotor Hub)

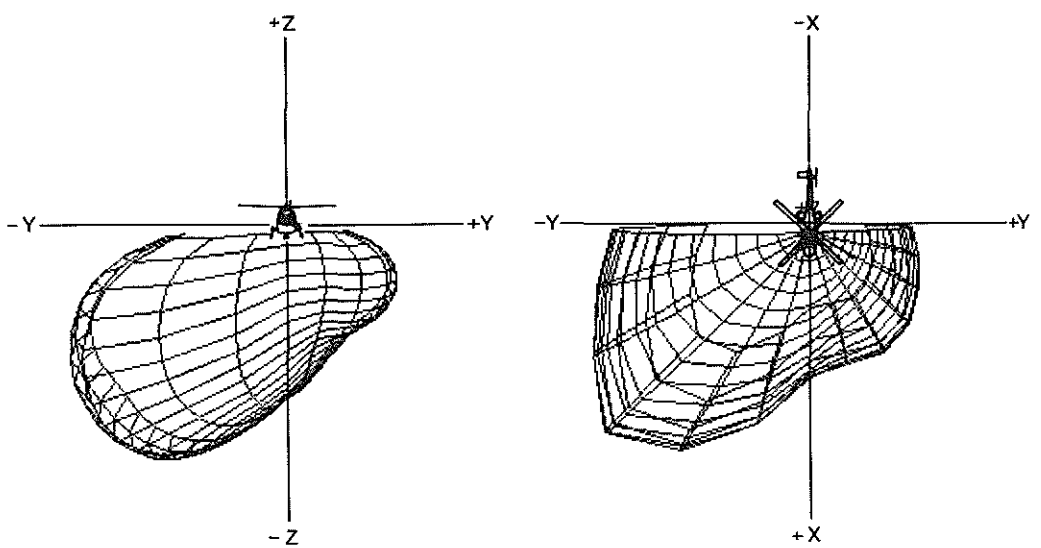

Figure 10 Predicted Directivity Patterns for 6°/70 Knot Condition Relative to Helicopter

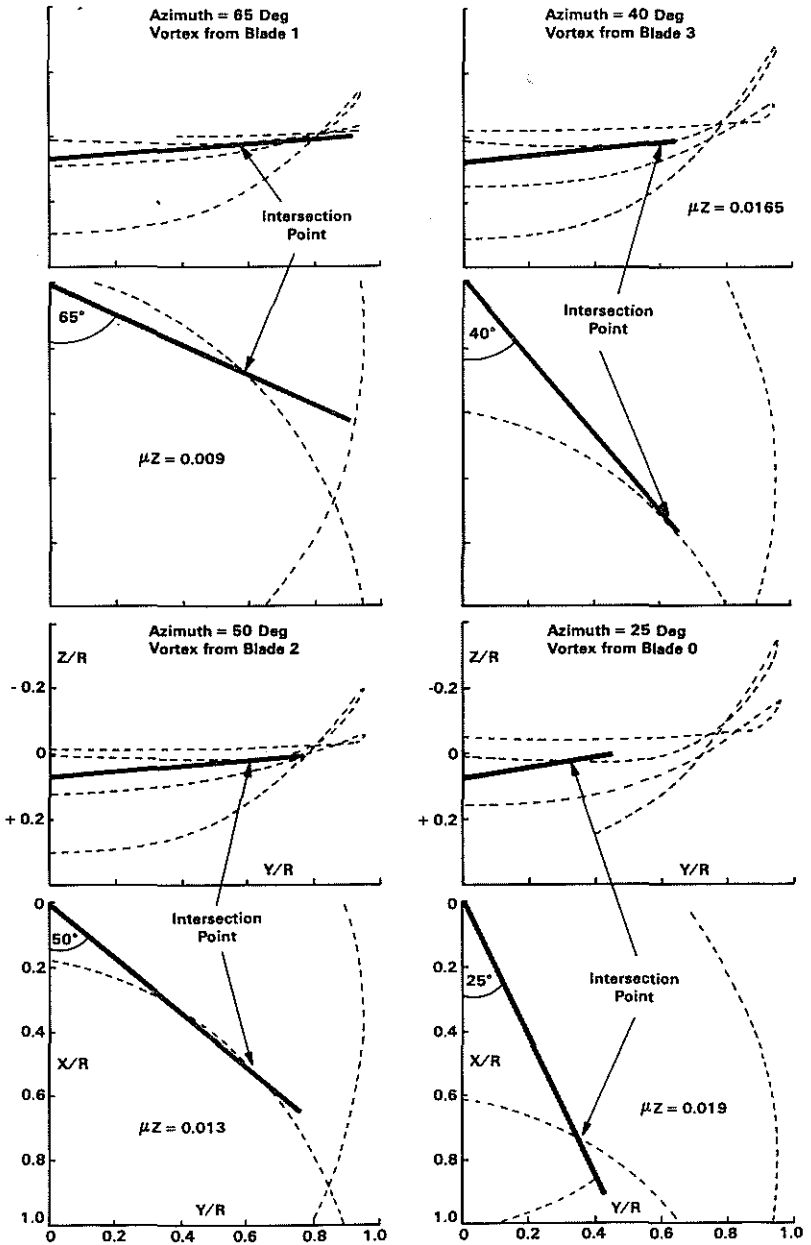

Figure 11 Vortex Paths Relative to Blade (70 Knots)

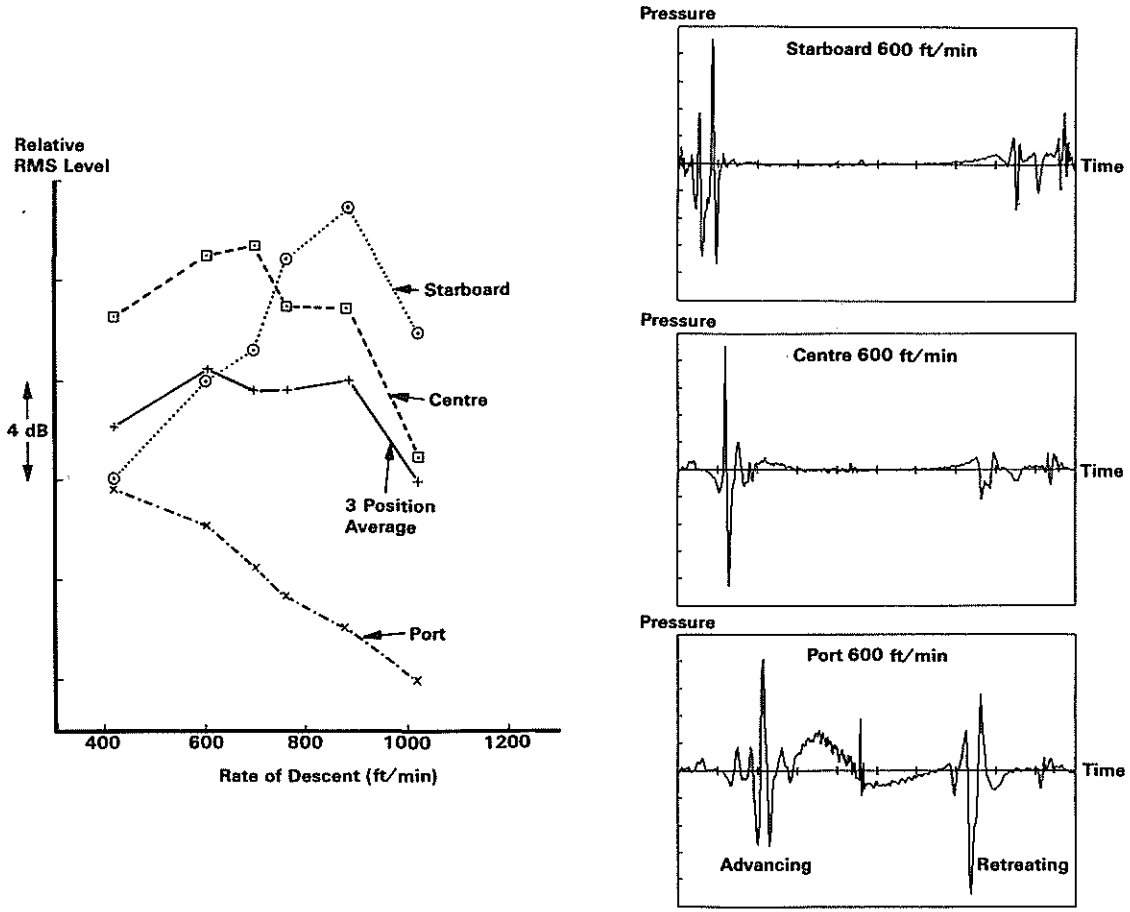

Figure 12 Predicted Level Variation with Descent Rate at 70 Knots Forward Speed

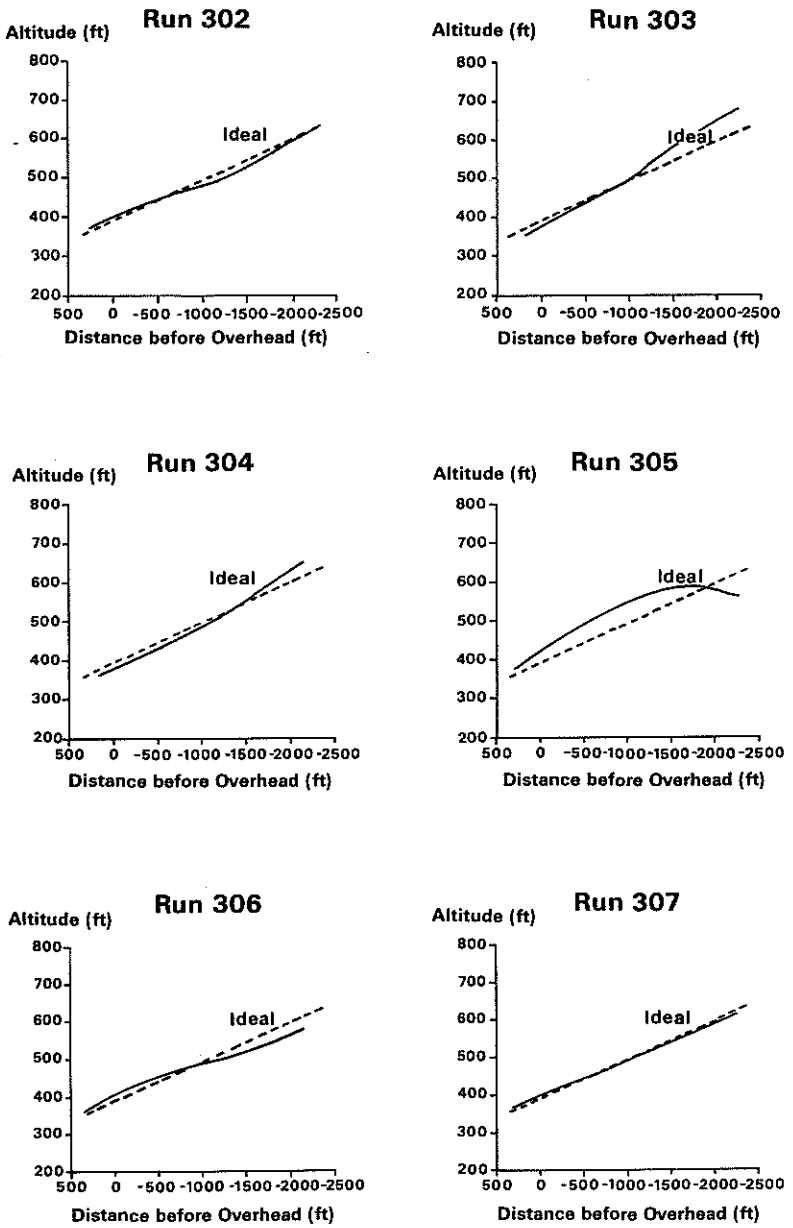

Figure 13 Measured Flight Paths for Nominal 6° Glide Slope

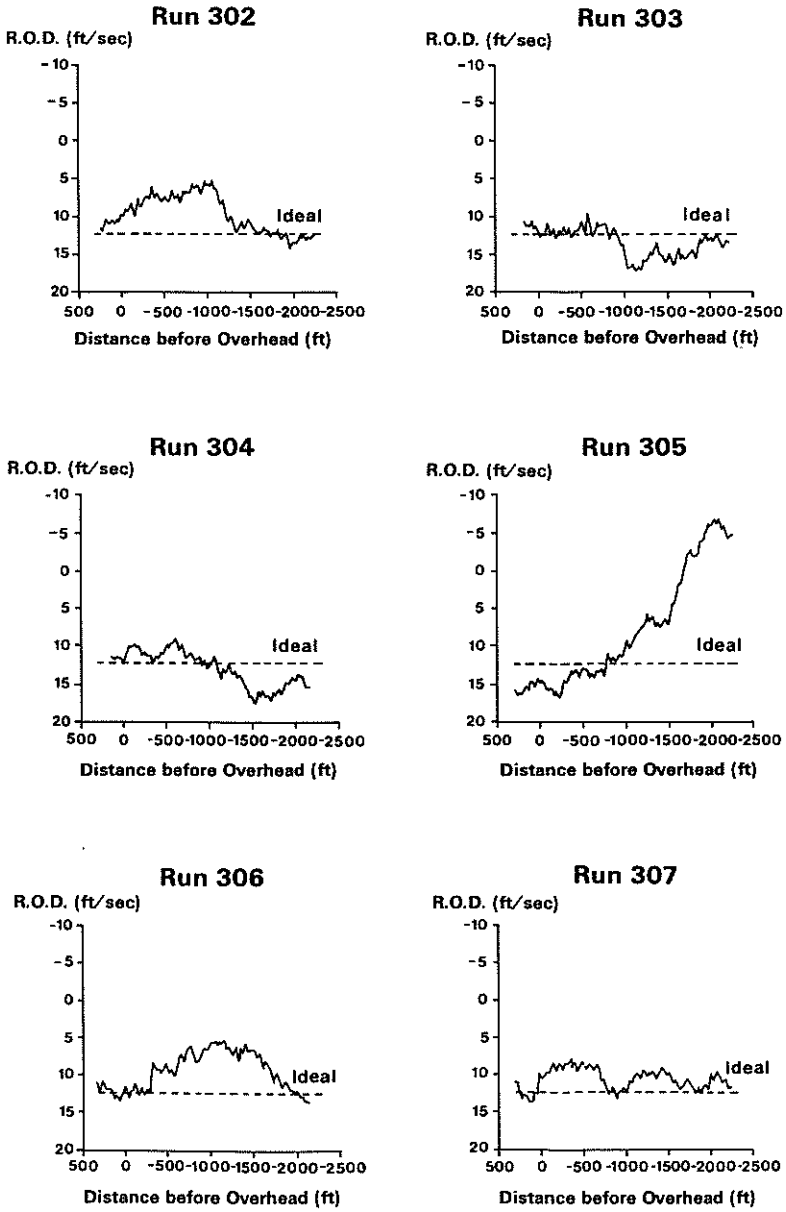

Figure 14 Measured Rates of Descent for Nominal 12.3 Ft/s (740 Ft/Min)

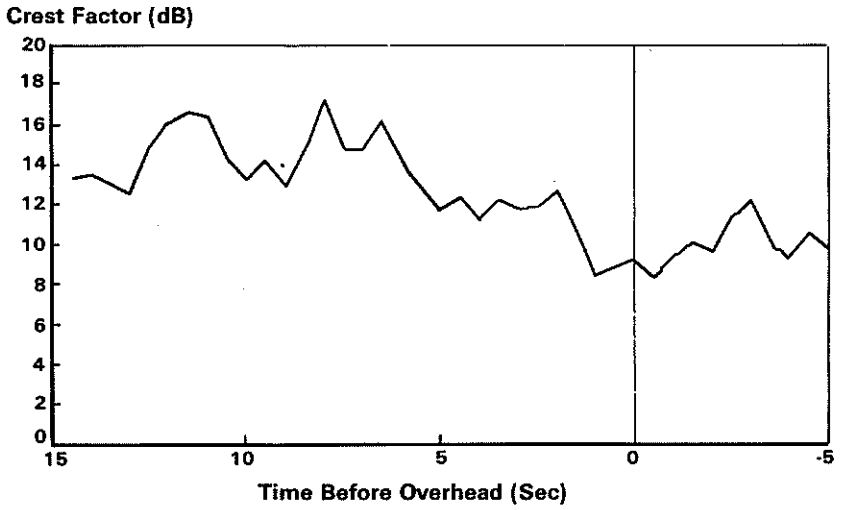

Figure 15 (a) Crest Factor Time History For Run 304

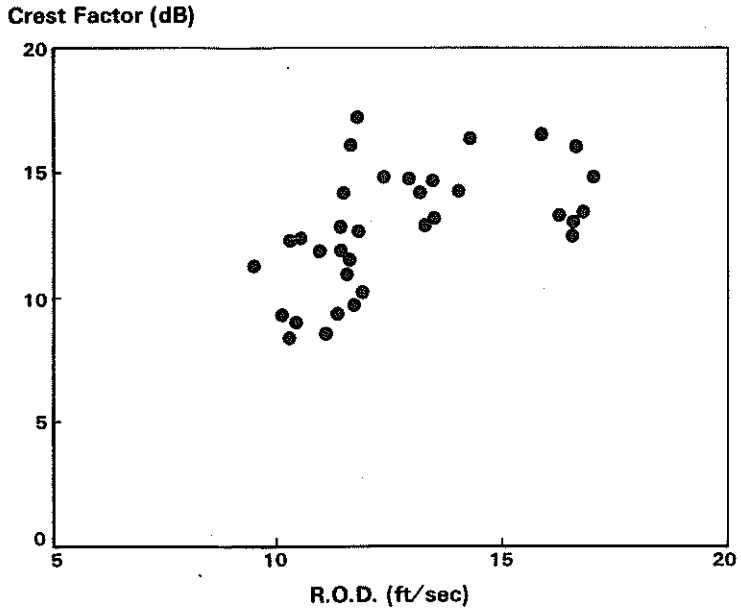

Figure 15 (b) Crest Factor Correlation with Descent Rate (Run 304)

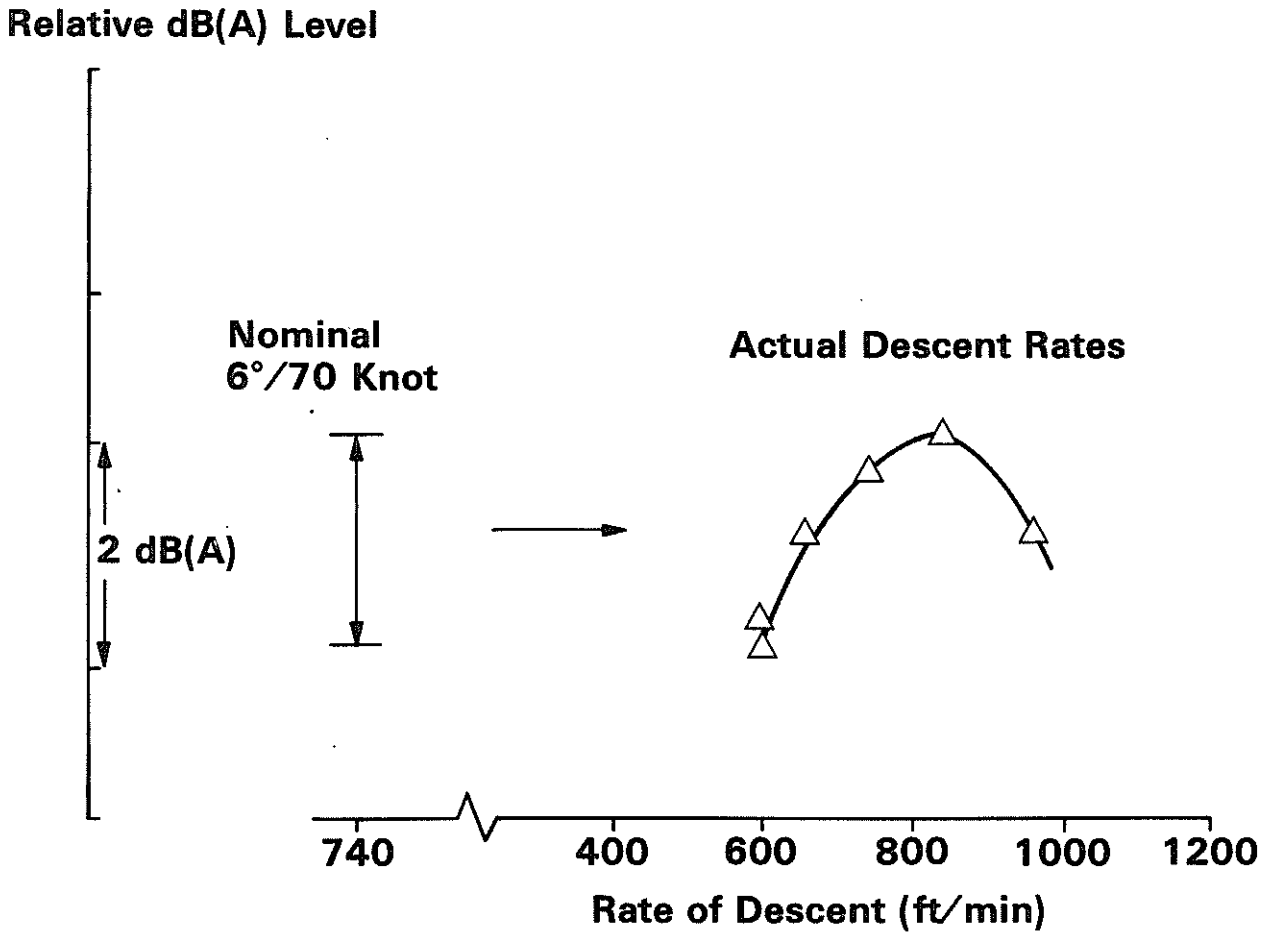

Figure 16 Effect of Correcting for Actual Descent Rates During I.C.A.O. Certification Trial (Runs 302-307)